# CHAPTER III
EXPERIMENTAL PROCEDURE

Chapter III presents the experimental procedures of this research. The detailed steps are outlined in the following sections.

3.1 Synthesis of β–Zn$_4$Sb$_3$ powders

The β–Zn$_4$Sb$_3$ powders were prepared through a solid–state reaction and calcination under a flow of Ar gas. Initially, elemental powders of Zn [99.9%, Alfa AesarTM] and Sb [99.5%, Sigma–Aldrich] were prepared in a stoichiometric ratio 4:3 with with excess Zn powders conditions. The premixed powders were weighted to 10 g for each Zn–rich condition. The excess Zn rich was added to compensate for any losses of Zn elements due to evaporation during high temperatures calcination (Ur et $al.$, 2003). The premixed powders, along with 2 mm zirconia balls, were placed into a 125 ml polypropylene (PP) cylindrical bottle, with zirconia balls filling approximately 75% of the PP bottle's volume. Then, the filled PP bottle was rotated at a maximum speed of 700 rpm using a roller milling machine for 24 hours. After milling, the Zn-Sb powder mixture was calcined under an Ar gas flow, which was passed through a water jar serving as an air barrier. The heating rate was set to 10 ℃/min until the target temperature was reached, where it was then held steady for specified time conditions. Finally, the mixture was allowed to cool to room temperature. An illustration of the process synthesis is shown in Figure 36. The series of synthesis conditions of β–Zn$_4$Sb$_3$ powders is presented in Table 4. These conditions were tested to compare the crystallite phases of β–Zn$_4$Sb$_3$ in order to determine the optimal synthesis conditions.
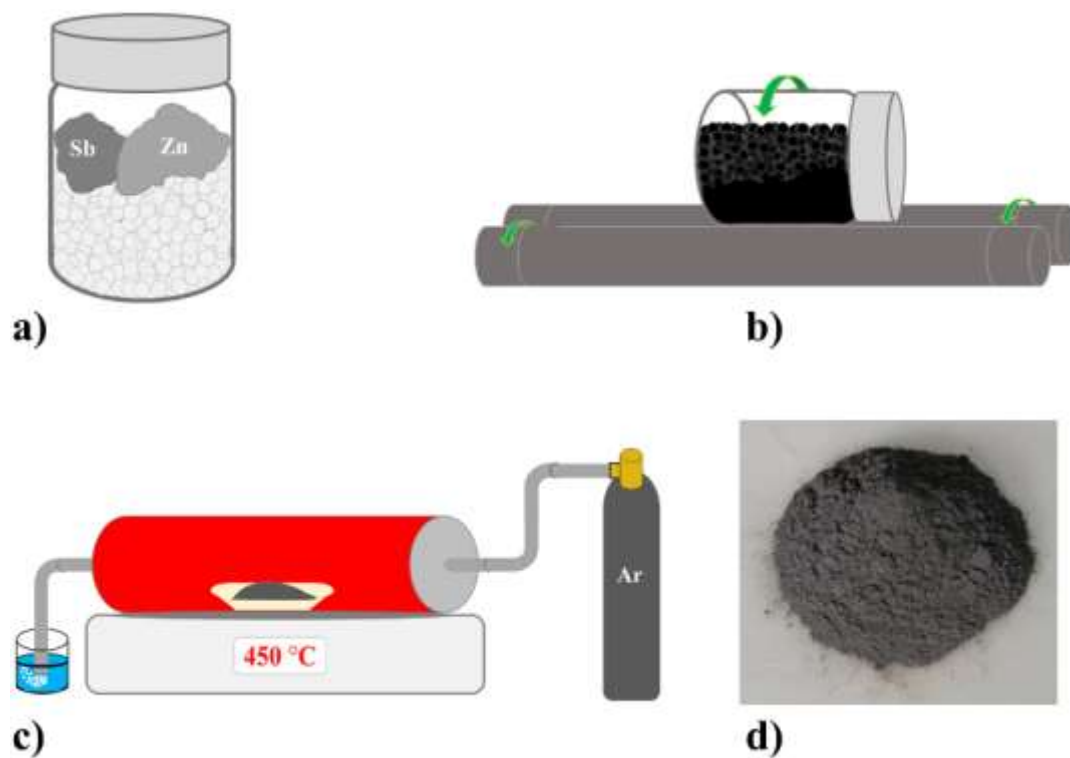
Figure 36 Process synthesis of β–Zn_4Sb_3 powders: a) Premixed powders with zirconia balls were filled into a PP bottle, b) The filled PP bottle was rotated using roller milling machine, c) The mixture powders were calcined under Ar gas flow, and d) Synthesized β–Zn_4Sb_3 powders.

Table 4 Series conditions of process synthesis of β–Zn_4Sb_3 powders versus excess Zn, calcination temperature and calcination holding time.

Excess Zn (at.% Zn)	Calcination Temp.	Holding time (hour)
0	Non cal., 300 °C, 400°C, 500°C	3
0, 5, 10, 15, 20	400 °C	3
10	400 °C	1, 3, 5
10	350 °C, 400 °C, 450 °C	3
10–14	400 °C	3
10–14	450 °C	3
10–14	500 °C	3

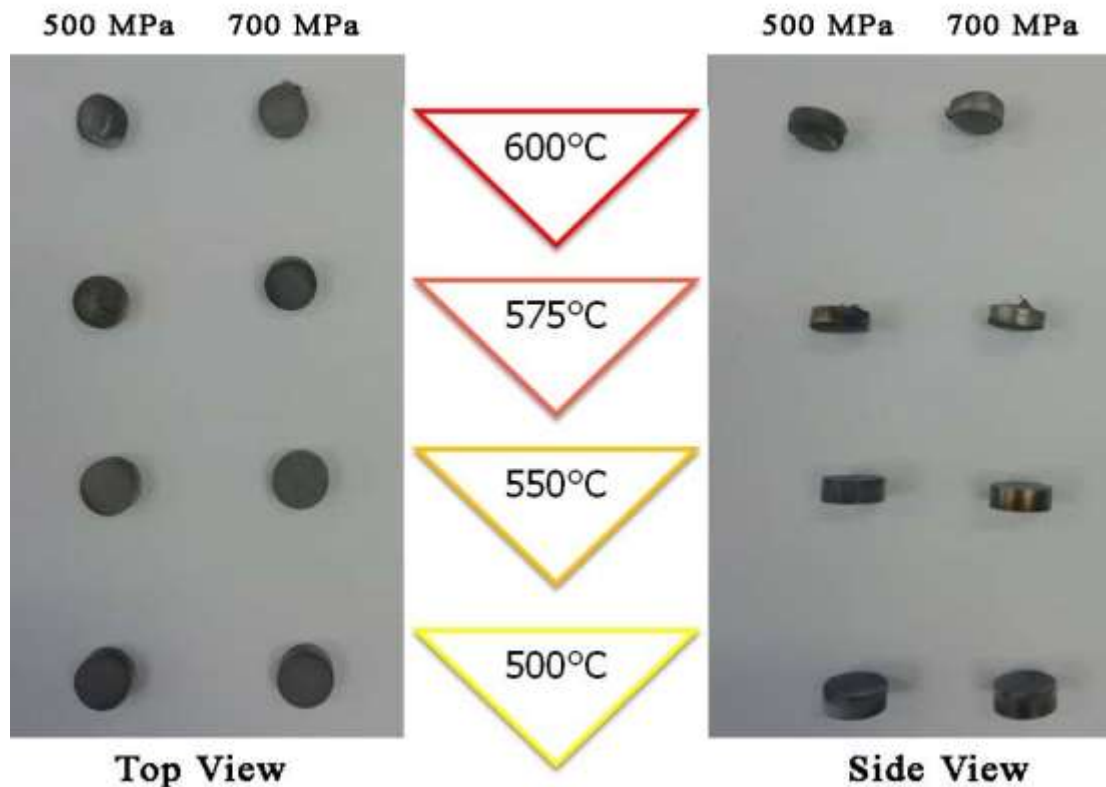## 3.2 Fabrication of sintered β–Zn_4Sb_3 pellets

The synthesized β–Zn_4Sb_3 powders were filled into a circular compression mould with a hole diameter of 1 cm. The mold was pressed to pressures of 500 MPa and 700 MPa, held for 15 minutes. The high compression pressure directly increased the density of the pellets, as shown in Table 5 (Lee and Lin, 2018). The maximum pressure of our hydraulic equipment is 700 MPa with 500 MPa used for comparison. As shows in Figure 37, the pressed β–Zn_4Sb_3 pellets were sintered under Ar gas flow at a heating rate 1 °C/min until the target temperatures of 500 °C, 550 °C, 575 °C and 600 °C were reached. The pellets were held at these temperatures for 6 hours and then allowed to cool to room temperature. Finally, the successfully sintered β–Zn_4Sb_3 pellets are depicted in Figure 38.

Table 5 Pressure in compression process with calculation density of pressed β–Zn_4Sb_3 pellets.

Materials	Diameter (cm)	Pressure (tons/MPa)	Thickness (cm)	Density % (g/cm^3)
β–Zn_4Sb_3	1.0	4.6/500	3.7	83
β–Zn_4Sb_3	1.0	5.6/700	3.6	86
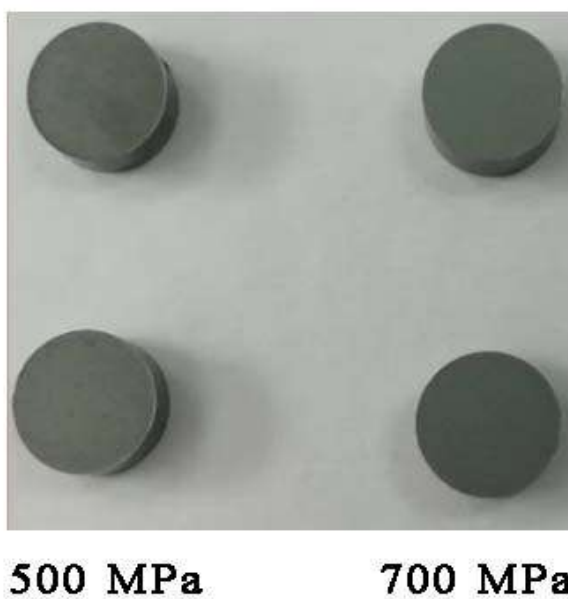
Figure 37 The β–Zn_4Sb_3 bulk pellets after were pressed at 500 and 700 MPa, respectively.

Figure 38 The sintered β–Zn_4Sb_3 pellets after were sintered at 500 °C, 550 °C, 575 °C and 600 °C for 6 hours.

Based on the experimental results, the optimal condition for fabricating the sintered β–Zn_4Sb_3 pellets is a compression pressure of 700 MPa. The pellets sintered at compression pressure 700 MPa and a temperature of 550 °C showed good durability, although some swelling was observed at the rims. To refine the process further, sintering at 525 °C was also explored under the same 700 MPa compression. As a result, sintered β–Zn_4Sb_3 pellets were produced under condition of 700 MPa with sintering temperature at 500 °C, 525 °C and 550 °C.

3.3 Fabrication of test cells monolithic β–Zn$_4$Sb$_3$ /ZnO TEG module

Innitially, the synthesized β–Zn$_4$Sb$_3$ powders were filled into a square compression mold size 1x1 cm with a weight of 0.2 g and gently pressed at 100 MPa. Next commercial ZnO powders [99.9%, KemAus™] were added into the same mold for 0.2 g and gently pressed. The ZnO powders layers served as insulating plates due to the high electrical resistivity of ZnO materials (Jantrasee *et al.*, 2016). The soft compression process for the β–Zn$_4$Sb$_3$ and ZnO powders was repeated twice. Afterward, the combined β–Zn$_4$Sb$_3$ and ZnO powders was firmly hard pressed at 700 MPa for 15 minutes. The compression process is depicted in Figure 39. The pressed β–Zn$_4$Sb$_3$/ZnO pellets were sintered by gradually increasing the temperature at a rate of 1 ℃/min under Ar gas flow until reaching 500 ℃, and held for 6 hours. Following the sintering process, the pellets were coated with ethyl cyanoacetate to strengthen the multi-stack structure. Electrical wires were then used to connect the two β–Zn$_4$Sb$_3$ layers in a zigzag configuration, forming a series circuit between the positive and negative terminals. To protect against lead solder melting during operation at 300 ℃, the top and bottom of the test cells were covered with a cement filler. The above process was repeated using different initial weights of β–Zn$_4$Sb$_3$ powders for 0.5 g, 1 g, 2 g and 4 g, to compare the open-circuit voltage, IV characteristics, and electrical power output, with the goal of identifying the optimal starting weight for the fabrication of monolithic multi-stack β–Zn$_4$Sb$_3$/ZnO TEG modules. Finally, the monolithic β–Zn$_4$Sb$_3$/ZnO TEG test cells were successfully fabricated, as shown in Figure 40.
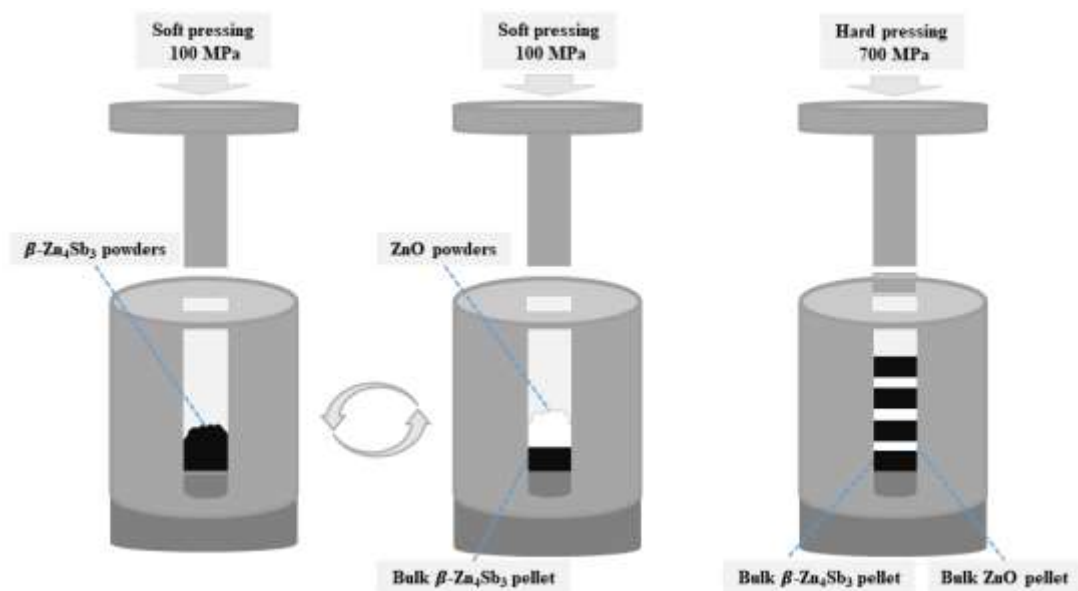
Figure 39 The cyclical compression process for preparing β–Zn_4Sb_3/ZnO pellets.

Figure 40 The test cells of monolithic β–Zn_4Sb_3 /ZnO TEGs versus weight size of β–Zn_4Sb_3 pellets part.

3.4 Fabrication of monolithic multi–stack β–Zn$_4$Sb$_3$/ZnO TEG module

This fabrication process is similar to that of the test cells, but with the soft compression method of β–Zn$_4$Sb$_3$ powders and ZnO powders repeated multiple times. Afterward, the multi-stack layers of multi–stack of β–Zn$_4$Sb$_3$ and ZnO powders was firmly hard pressed at 700 MPa for 15 minutes. The compression processes is depicted in Figure 39. The pressed multi–stacks β–Zn$_4$Sb$_3$/ZnO pellets were sintered by gradually increasing the temperature at a rate of 1 °C/min under Ar gas flow until reaching 500 °C, and held for 6 hours. After sintering, the multi–stacks β–Zn$_4$Sb$_3$/ZnO pellets were coated by ethyl cyanoacetate to enhance its strength. Then the β–Zn$_4$Sb$_3$ layers of the multi-stack pellet were then connected with electrical wires in a zigzag configuration to form a series circuit between the positive and negative terminals. To protect against lead solder melting during operation at 300 °C, the top and bottom of the multi-stack β–Zn$_4$Sb$_3$/ZnO TEGs were coated with a cement filler. Finally, the monolithic multi–stack β–Zn$_4$Sb$_3$/ZnO TEGs were successfully fabricated, as shows in Figure 41.
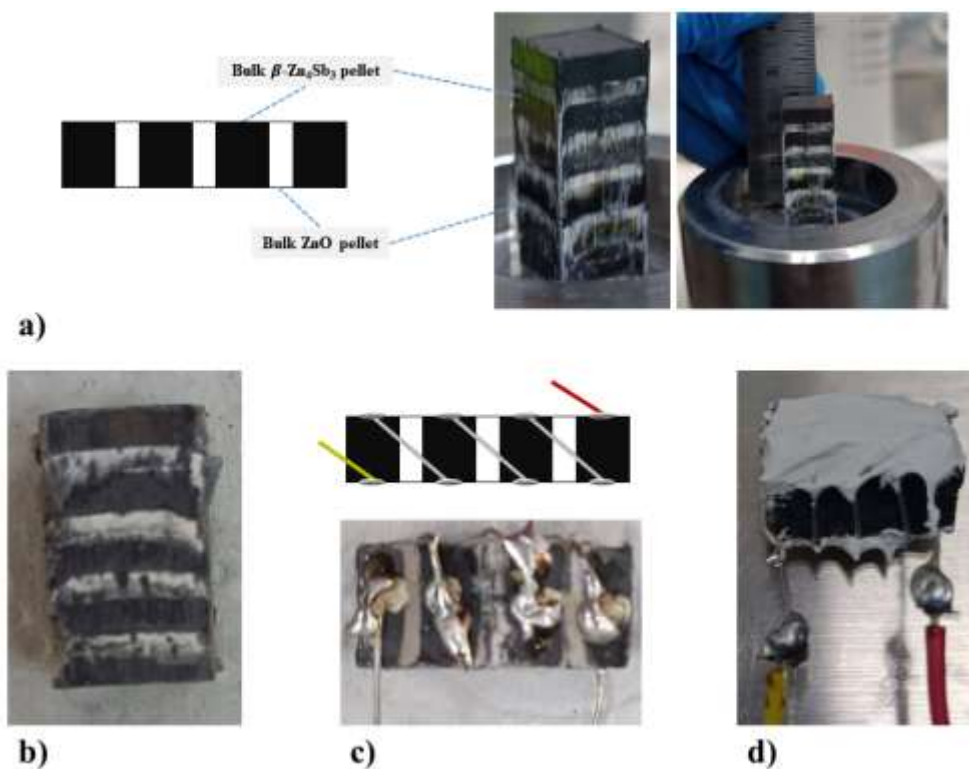
Figure 41 Fabrication processes of monolithic β–Zn$_4$Sb$_3$/ZnO TEGs: a) compressed multi–stacks β–Zn$_4$Sb$_3$/ZnO pellet, b) sintered multi–stacks β–Zn$_4$Sb$_3$/ZnO pellet, c) connected electrical wire with zigzags connection of monolithic β–Zn$_4$Sb$_3$/ZnO TEGs, and d) monolithic β–Zn$_4$Sb$_3$ TEGs was plastered with cement filler.

3.5 Materials characterization

In this work, the β–Zn$_4$Sb$_3$ sample was analyzed crystallite structure, local oxidation of component elements, and the binding energy of materials elements. The details of the technical characterizations and methods are outlined in the following subtopics.

3.5.1 X–ray diffraction

The crystallite structure of β–Zn$_4$Sb$_3$ was investigated using X–ray diffraction technique (D8–Bruker). The X–ray diffraction technique (D8–Bruker) is shown in Figure 43. The XRD technique was employed to determine the crystallite structure pattern of β–Zn$_4$Sb$_3$, and the resulting diffraction patterns were compared with Mozharivskyj's model (Mozharivskyj *et al.*, 2006). However, the X–ray diffraction for all samples revealed the presence of a secondary phase. The fundamental principle of X–ray diffraction is based on Bragg's law scattering, which describes how X-rays interfere through constructive and destructive interference with each other beam, depending on the diffraction angles. This correlation are explained by following equation.

$$2d\sin\theta = n\lambda \tag{113}$$

Where d is space between crystallite plan, θ is an angle of incident X–ray beam, λ is X–ray wavelength, which the wavelength is 0.15406 nm, and n is the order of the X-ray interference beam, along with destruction and construction.

the intensity and width of the X-ray diffraction patterns can be used to calculate the crystallite sizes of the samples. However, this study did not focus on crystallite size. Crystallite sizes are typically calculated using the Debye-Scherrer equation, as shows in equations (114).
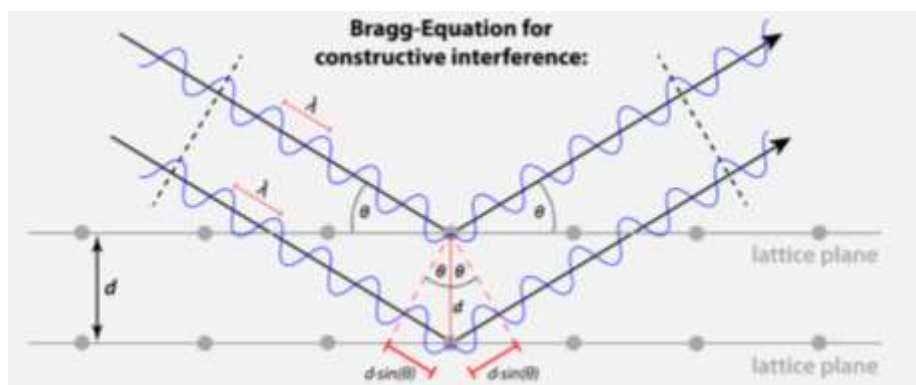
$$D = \frac{k\lambda}{\beta\cos\theta} \tag{114}$$

Where;

D is a crystallite size

k is a spherical factor, which the factor is $k \approx 0.9$

β is a full width half maximum *(FWHM)* intensity of x–ray diffraction peaks.

Figure 42 Shows x–ray incident and diffraction, according to Bragg's law (www.didak tik .physik.uni–muenchen.de/elektronenbahnen/en/index.php).

Figure 43 Shows X–ray diffraction machine, D8–Bruker, SUT.

3.5.2 X–ray absorption spectroscopy

X–ray absorption spectroscopy (XAS) is a technique used to studied near–edge structure of materials elements by analyzing X–ray absorption near–edge structure (XANES) spectra. This method investigates the ionization energy for exciting core electrons. The transmission intensities of the X–ray beam are measured to determine the ionization energy of core electrons, which reveals the oxidation state of local elements within the sample. Each electron orbital and absorption edge absorb specific X–ray energies, as illustrated in Figure 44. Therefore, the X–ray absorption spectra of the electron orbitals provide insight into the material's structure. Typically,

the X–ray absorption measurement are conducted in transmission mode for bulk samples, as shown in Figure 45. The intensity of the transmitted X–ray beam relative to the incident X-ray beam intensity is expressed as a function of the X-ray absorption coefficient μ(E), represented by the following (115).
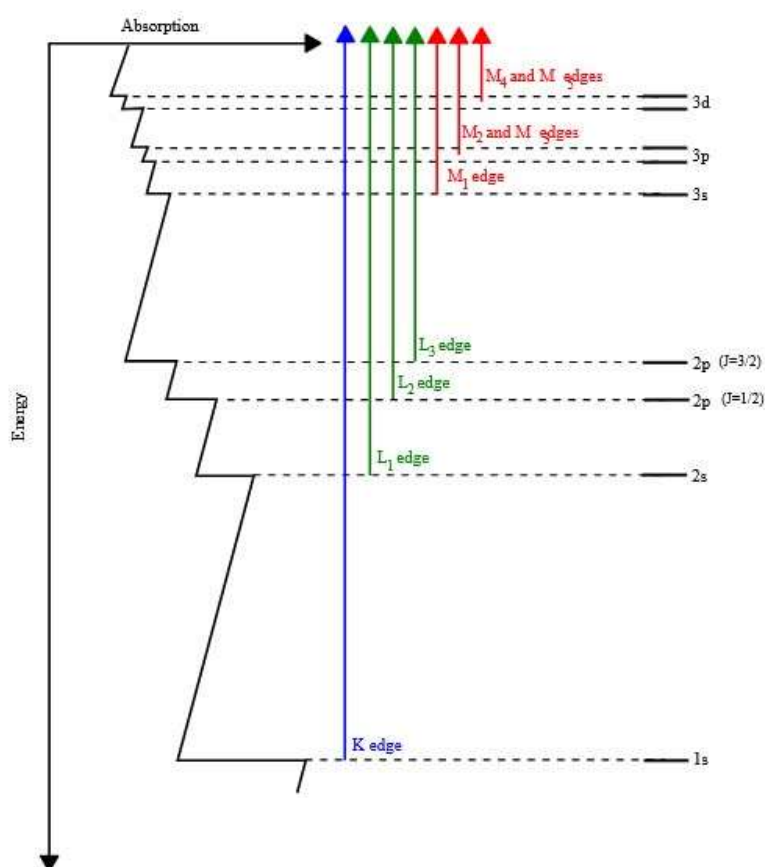
$$\mu(E)t = -\ln \frac{I}{I_0} \tag{115}$$

Where;

μ_E is absorption coefficient.

I is x–ray transmission intensity

I_0 is x–ray incident intensity.

t is sample thickness.

The XANES measurement technique as transmission mode is shown in Figure 45.

Figure 44 Illustration of a x–ray absorption energies of K edge, L edges and M edges (Chem.libretexts, 2000).
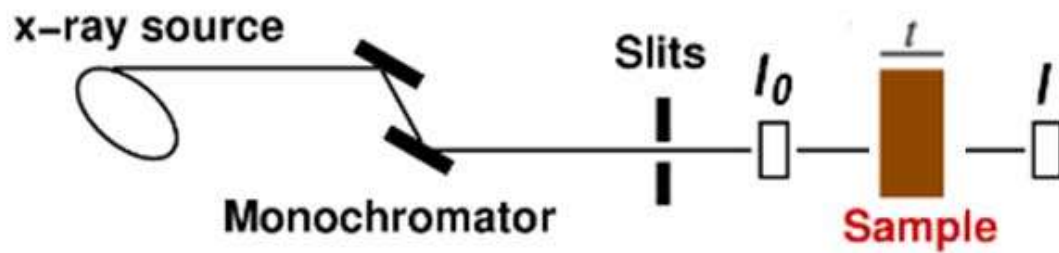
Figure 45 Illustration of x–ray absorption transmission mode (Mit.edu, 2004).

3.6 Thermoelectric properties

The thermoelectric properties of materials include the Seebeck coefficient, electrical conductivity, electrical power factor, and thermal conductivity. In this research, the commercial Linseis LSR–3 equipment was used to measure these properties. This equipment operates based on the principle of thermoelectric measurement (Goldsmid, 2010), where it measures the voltage (V) as a function of the temperature gradient across the sample, as you know Figure 46.
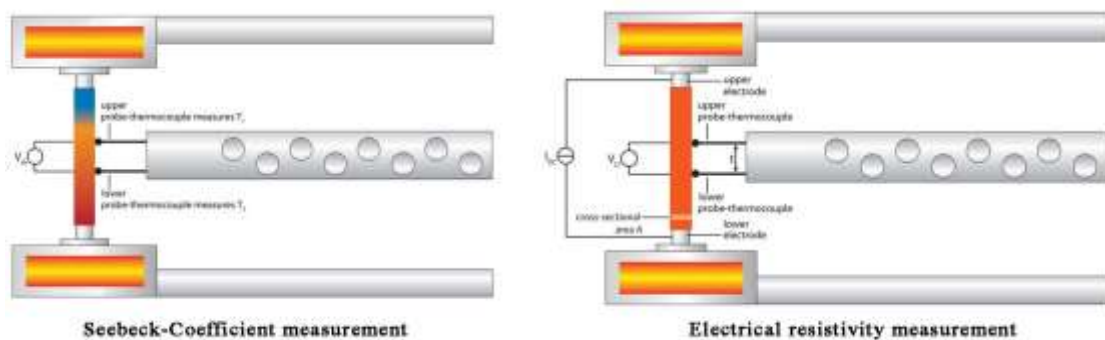

Figure 46 Illustration of Seebeck coefficient and electrical resistivity (Linseis, 2024).

Figure 47 LINSEIS LSR–3 Seebeck type resistivity measurement system.

3.7 Module evaluation

Due to limitations of commercial equipment for evaluating IV–curves and electrical output power curves of the TEG modules, a custom-built heating/cooling system with IV measurement capabilities was developed. The system is controlled by a temperature controller board, while the IV–curve was measured using a commercial current/voltage meter and a potentiometer. The setup is illustrated in Figure 48.
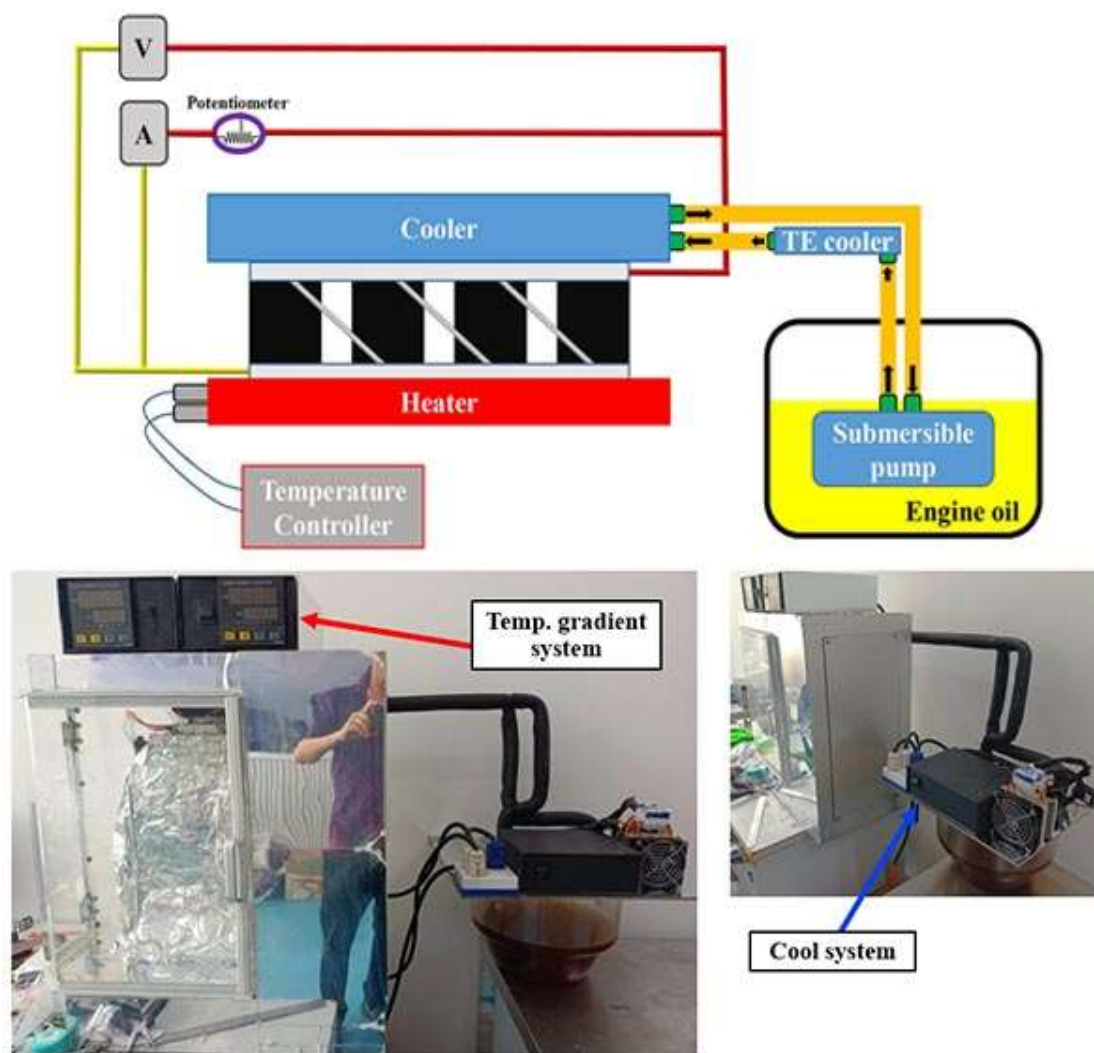
Figure 48 The self–made heating/cooling system with IV measurement capabilities.